

# Laser structuring of electrodes in roll-to-roll environment using multi-beam processing: process upscaling and its perspective

Alexandra P. Meyer<sup>\*a</sup>, Yannic Sterzl<sup>a</sup>, Ulrich Rädels<sup>b</sup>, Shizhou Xiao<sup>c</sup>, Manuel Zenz<sup>d</sup>, Daniel Schwab<sup>e</sup>, Wilhelm Pfleging<sup>a</sup>

<sup>a</sup> Institute for Applied Materials – Applied Materials Physics (IAM-AWP), Karlsruhe Institute of Technology, Hermann-von-Helmholtz-Platz 1, 76344 Eggenstein-Leopoldshafen, Germany; <sup>b</sup> Topag Lasertechnik GmbH, Nieder-Ramstädter Str. 247, 64285 Darmstadt, Germany; <sup>c</sup> EdgeWave GmbH, Carlo-Schmid-Straße 19, 52146 Würselen, Germany; <sup>d</sup> Sill Optics GmbH & Co. KG, Johann-Höllfritsch-Str. 13, 90530 Wendelstein, Germany; <sup>e</sup> Novanta Inc., 125 Middlesex Turnpike, Bedford, MA 01730, USA

## ABSTRACT

The development of next-generation lithium-ion batteries with volumetric energy densities  $> 750$  Wh/L and gravimetric energy densities  $> 400$  Wh/kg is a key objective of the European Union's Strategic Energy Technology Plan to be achieved by 2030. Both new materials and production strategies play an important role in the development of those batteries. Thick-film electrodes are advantageous to increase the volumetric and gravimetric energy densities alike since the amount of inactive material can be reduced. To facilitate higher C-rates during (dis-)charging in thick-film electrodes, laser generated structured are introduced, thus creating new lithium-ion diffusion pathways leading to a reduced cell polarization. Additionally, electrode wetting with liquid electrolyte is significantly improved, reducing the risk of dry spots in the electrode stack.

Industry interest in implementing laser patterning of electrodes into existing or planned manufacturing lines has increased significantly in recent times. The strip speeds of electrode production are decisive for the required speeds to be realized in laser structuring. Various technical approaches can be applied to upscale the laser patterning process such as multibeam processing which can be realized by splitting a laser beam into several beamlets with a DOE. In this work, a large field scanner and a related optical lens system are combined with an ultrashort pulsed, high repetition rate, high power laser source. The ablation behavior of commercial graphite composite electrode material was investigated for upscaling using different laser patterning scenarios.

**Keywords:** Ultrafast laser ablation, roll-to-roll processing, anode, lithium-ion battery, upscaling, laser structuring

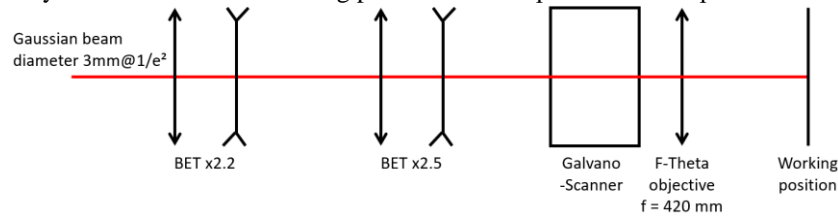
## 1. INTRODUCTION

One of the main approaches to decrease greenhouse gases emission and stop the pollution of the environment for the fulfillment of the climate-neutrality goal of the European Union [1] is the electrification of individual and goods transportation with electric vehicles (BEV), where lithium-ion batteries (LIB) provide the needed energy. The decentral conversion of energy in sun, wind, and water power plants in combination with stationary LIB energy storage facilities to realize peak shaving is another promising approach. State-of-the-art LIBs already have relatively high energy and power densities, as commercial cells, e.g., in the Volkswagen ID.3, have an energy density of 674 Wh/L and a specific energy of 268 Wh/kg [2], but a further increase in energy and power density, electrochemical performance, lifetime as well as cost-effectiveness is aspired. For this purpose, state-of-the-art LIBs electrodes can be modified by laser patterning. The introduction of artificial porosity increases the wetting of the electrodes due to the capillary effect [3] and therefore decreases the need for warm ageing, which is a bottleneck in LIB production. The usage of advanced anode materials with the addition of silicon and higher compression during calendaring is facilitated [4], both of which increase the energy density. The power density is increased by laser patterning due to the increased active surface area and decreased overall tortuosity, which decreases the lithium-ion diffusion overpotential and facilitates higher charge and discharge rates [4]. For the application of laser patterning in the already established cell manufacturing line, high processing speeds need to be achieved. Depending on the manufactured electrodes' thickness, belt speeds of 10 m/min to 30 m/min [5] are

realized during conventional coating and drying, but higher velocities are aspired. During electrode coating with dry materials, i.e., without the addition of solvents like N-Methyl-2-pyrrolidone (NMP) or water, coating speeds of 1.2 m/min are achieved [5], while the coating speed of slurries with very low solvent content in the range of 10 wt.% to 15 wt.% with electron-beam curing is reported to be as high as 150 m/min to 300 m/min [5]. As a result, the process of laser patterning needs to be designed according to those requirements. The patterning design most appropriate for high processing speeds is a line pattern with a specified pitch, or a hole pattern where each hole is drilled with a single laser pulse, so that no additional acceleration and deceleration for each drilling position is needed. Very high scanning speeds with high precision are necessary, therefore laser scanners with very low jitter, low inertia, and high powers are needed. An alternating scanning strategy with “skywriting” needs to be implemented as well. The laser source used for electrode patterning should have pulse lengths in the fs or ps range, as it was reported that the heat affected zone (HAZ) can be decreased and the quality of the grooves is increased compared to laser sources with pulse lengths in the ns range [4]. When a very high-power laser source is used, ordinary beam splitters or diffractive optical elements for beam splitting can be implemented to increase the total number of laser beams and therefore parallelize the processing, which increases the process speed immensely. Additionally, beam shaping optics can be implemented to increase the illuminated area and therefore facilitate even higher scanning and process speeds. This approach was followed in the presented publication.

## 2. EXPERIMENTAL

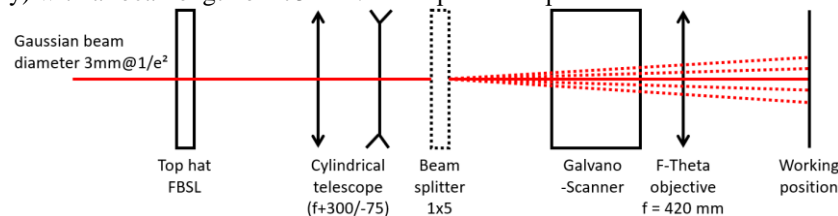
The laser patterning is realized by using a pulsed Yb:YAG solid-state laser system (FX600-2-GFH, Edgewave GmbH, Würselen, Germany) with InnoSlab© technology with a fundamental wavelength of 1030 nm, a pulse duration of 600 fs, and a pulse repetition rate between 4.9 MHz and 48.80 MHz, which is adjustable with a seeder frequency divider (SFD) between 1 and 10. The beam radius at the laser exit  $w_A$  is approx. 1500  $\mu\text{m}$ . The diffraction coefficient  $M^2$  of the laser is 1.1. The beam path for the first set of experiments with conventional optics is shown in Figure 1. A 2-axis scan head and a F-Theta lens (S4LFT2430/328, Sill Optics GmbH & Co. KG, Wendelstein, Germany) with a focal length of 420 mm were used for the delivery of the beam to the working position. This experimental setup is called “S1”.



**Figure 1: Illustration representing the optical beam path of the laser beam in the first set of experiments “S1”. The raw beam diameter is 3mm@1/e².**

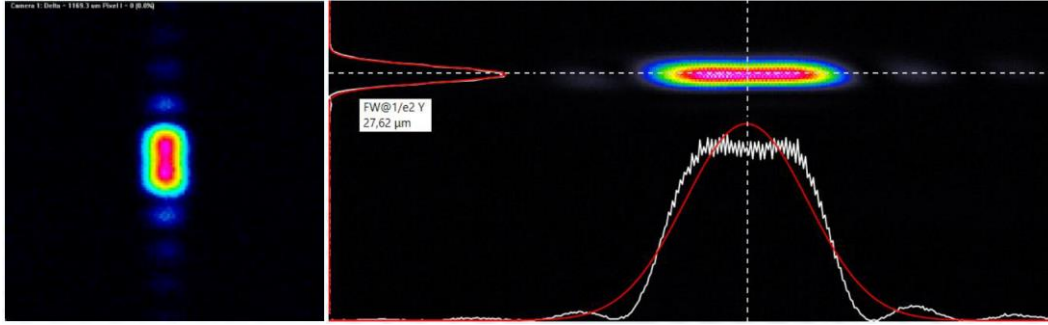
The beam path used for laser processing in the second set of experiments is shown in

Figure 2. A diffractive optical element (FBS-L©, TOPAG Lasertechnik GmbH, Darmstadt, Germany) is used to shape the beam into a one-dimensional top hat with a Gaussian intensity distribution in x-direction and a top hat shape in y-direction. Schematic intensity profiles of the shaped beam are shown in Figure 3. A cylindrical lens telescope was used to elongate the beam in y-direction. The telescope contained a plano convex lens (LJ1558RM-B, Thorlabs GmbH, Bergkirchen, Germany) with a focal length of 300 mm and a plano concave lens (LK1431RM-B, Thorlabs GmbH, Bergkirchen, Germany) with a focal length of -75 mm. This optical setup is referred to as “S2”.



**Figure 2: Illustration representing the optical path of the laser beam in the second and third set of experiments “S2” and “S3”, “S3” with dotted lines. The raw beam diameter is 3mm@1/e² and shaped to a top hat distribution along the y-axis.**

For some experiments, a beam splitter (DBS©, TOPAG Lasertechnik GmbH, Darmstadt, Germany) was also implemented, which is referred to as “S3”. The beam splitter divides the incoming beam into five beamlets with a separation angle of  $0.1385^\circ$ .



**Figure 3: Schematic intensity profiles of the shaped beam (©Topag AG).**

For the electrode material, commercial state-of-the-art double-sided graphite electrodes were used. They had a thickness of  $45.25 \pm 1.25 \mu\text{m}$  per side.

Several lines were manufactured in the electrode with one set of parameters, and the patterning results were examined using a digital microscope (VHX 5000, Keyence, Osaka, Japan) and a light microscope (Reicher-Jung MeF3, Leica Microsystems GmbH, Wetzlar, Germany) regarding the widths and depths of the channels and a scanning electron microscope (Phenom XL, Thermo Fisher Scientific Inc., Waltham, USA), where the overall topography, emerging cracks and debris formation were of interest. The different repetition rates and assigned scan speeds used in “S1” are summarized in Table 1. Average laser powers between 12 W and 240 W were applied.

**Table 1: Repetition rates and scan speed for each repetition rate applied in “S1”.**

Repetition rate /MHz <sup>(*)</sup>	Scan speed $v$ /mm s <sup>-1</sup>
48.8	5000
24.5	2500
16.3	1667
12.2	1250
9.8	1000
8.1	833
7.0	714
6.1	625
5.4	556
4.9	500

(\*) repetition rates (in MHz) are rounded to the first decimal place

For “S2” and “S3”, the repetition rate was kept constant at 4.9 MHz. Due to diffractive losses at the beam shaping and splitting optics, the total power was limited to 150 W, i.e., approx. 30 W per beam in “S3”. Different scanning velocities were applied between 0.5 m/s and 8.0 m/s.

### 3. RESULTS AND DISCUSSION

#### Evaluation of the laser patterning manufactured with “S1”

Figure 4 a) shows the semi-logarithmic plot of the ablation depth as a function of the pulse peak fluence for the patterned anode. A transition in the ablation behavior, characterized by a change in the slope, can be identified at approx.  $0.3 \text{ J/cm}^2$ . For the laser drilling of metals, this change in slope has already been observed by Nolte et al. [6]. Two ablation regimes can be identified. While ablation without thermal influence dominates at low laser fluences, the thermal influence at the ablation behavior cannot be neglected at higher fluences. Even though the ablation behavior for laser drilling cannot be directly transferred to direct-write ablation, since the locally applied fluences are not constant due to the pulse offset and the Gaussian distribution of the laser intensity, a similar behavior is observed here.

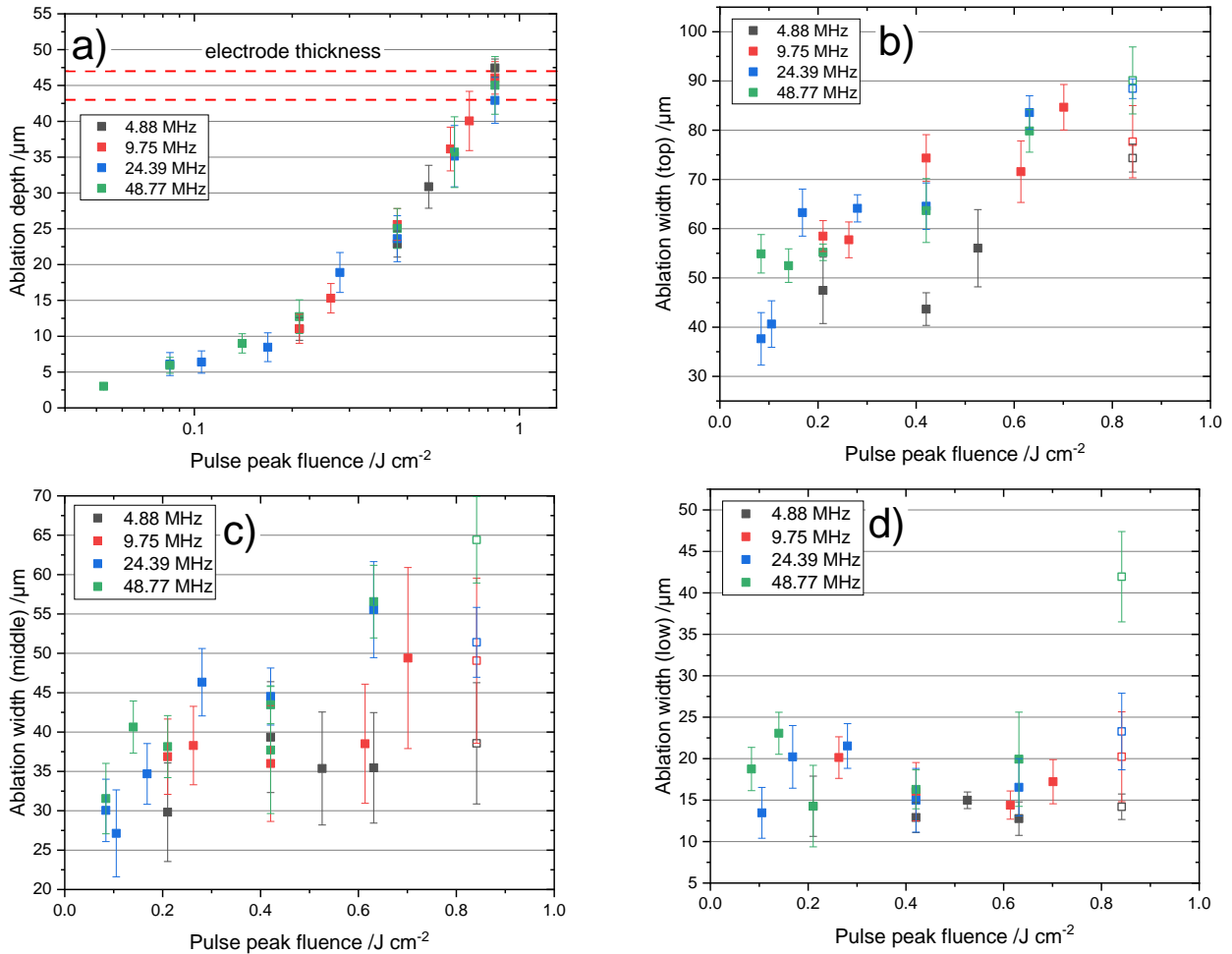


**Figure 4: a) Ablation depth b) upper ablation width c) middle ablation width and d) lower ablation width of the kerfs for the repetition rates of 4.9 MHz, 9.8 MHz, 24.4 MHz and 48.8 MHz and the laser scanning speeds of 500 mm/s, 1000 mm/s, 2500 mm/s and 5000 mm/s, respectively. Solid symbols: current collector was not reached, open symbols: current collector was reached.**

An influence of the repetition rate on the ablation depth is not evident. From a pulse peak fluence greater than  $0.70 \text{ J/cm}^2$ , the current collector is reached for all repetition rates. For the channels which were patterned with a repetition rate of 48.8 MHz and a pulse peak fluence of  $0.84 \text{ J/cm}^2$ , the current collector is already slightly damaged.

The measurement of the upper, middle, and lower widths, shown in Figure 4 b) to d) proved to be difficult. The structures show a strong scatter in their width, and the standard deviation for example of the measured upper ablation width assumes values of over  $8 \mu\text{m}$ . The ablation widths do not increase continuously with the pulse peak fluence for all the repetition rates, but in some cases decreases or remain at the same level. The upper ablation width as a function of the pulse peak fluence is shown in Figure 4 b). The curve flattens with increasing pulse peak fluences. The upper ablation widths are in the range of the film thickness ( $45.25 \pm 1.25 \mu\text{m}$ ) even at low pulse peak fluences of less than  $0.2 \text{ J/cm}^2$ . For all pulse peak fluences, where data is provided, the lowest ablation widths are obtained for a repetition rate of 4.9 MHz. The scatter in the upper ablation width can be seen by the large standard deviations. For a pulse peak fluence of  $0.21 \text{ J/cm}^2$ , the upper ablation widths for all measured repetition rates range from  $47 \mu\text{m}$  to  $55 \mu\text{m}$ . The highest upper ablation width for  $0.21 \text{ J/cm}^2$  is measured at 9.75 MHz with  $58.5 \pm 3.1 \mu\text{m}$ . From a pulse peak fluence equal to or greater than  $0.84 \text{ J/cm}^2$ , a continuous increase in ablation width with repetition rate can be seen, with the ablation width reaching  $90.1 \pm 6.8 \mu\text{m}$  at 48.8 MHz.

When considering the ablation width in the middle of the structures (Figure 4 c)), no statement can be made about a dependence of the mean ablation width on the pulse peak fluence due to the scatter. The same applies to the lower width

(Figure 4 d)), where the scatter in the ablation width also does not allow any statement about the behavior above the pulse peak fluence. It is striking that the mean ablation widths increase with the repetition rate at a pulse peak fluence of  $0.84 \text{ J/cm}^2$ .

The lower width plotted against the pulse peak fluence is shown in Figure 4 d). The lower ablation widths have values between  $12 \text{ }\mu\text{m}$  to  $23 \text{ }\mu\text{m}$ . For the lower ablation widths at  $48.8 \text{ MHz}$ , an increase is shown with reaching the current collector. The highest lower ablation width values of  $42.0 \pm 5.4 \text{ }\mu\text{m}$  are measured at a repetition rate of  $48.8 \text{ MHz}$  and a pulse peak fluence of  $0.84 \text{ J/cm}^2$ . No broadening of the structures near the current collector at a pulse peak fluence of  $0.84 \text{ J/cm}^2$  and a repetition rate of  $4.9 \text{ MHz}$  can be observed, while at  $48.8 \text{ MHz}$  the lower width at the current collector increases significantly.

In Figure 5 a), the aspect ratio is plotted against the pulse peak fluence at a constant repetition rate. The aspect ratio increases with increasing pulse peak fluence. There is no significant decrease in aspect ratio when the current collector is reached. The aspect ratio is always higher or at the same level with increasing pulse peak fluence for a constant repetition rate.

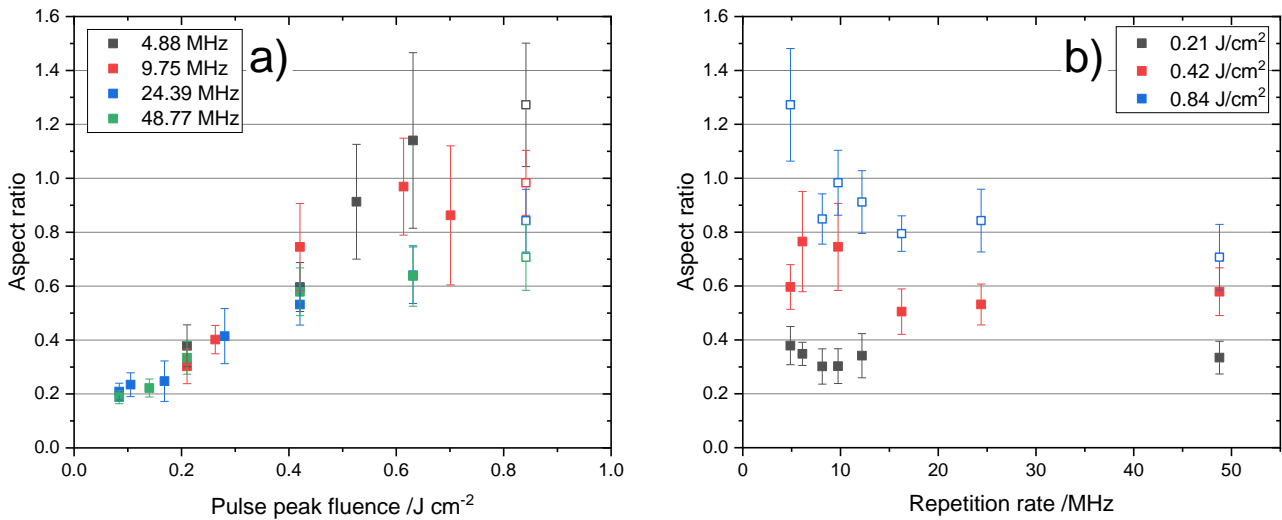


**Figure 5: a) Aspect ratio depending on pulse peak fluence for constant repetition rates b) aspect ratio depending on repetition rate for constant fluences. Solid symbols: current collector was not reached, open symbols: current collector was reached.**

The aspect ratio as a function of the repetition rate at constant pulse peak fluence is shown in Figure 5 b). At a pulse peak fluence of  $0.84 \text{ J/cm}^2$ , at which the current collector is reached for all repetition rates, the aspect ratio decreases with increasing repetition rate. Thus, for structures generated with  $4.9 \text{ MHz}$  and  $0.84 \text{ J/cm}^2$ , the aspect ratio is  $1.3 \pm 0.2$  and decreases to  $0.7 \pm 0.1$  at  $48.8 \text{ MHz}$ . For pulse peak fluences equal to or smaller than  $0.42 \text{ J/cm}^2$ , the influence of repetition rate on aspect ratio decreases. At  $0.42 \text{ J/cm}^2$ , an aspect ratio of  $0.6 \pm 0.1$  is obtained at  $4.9 \text{ MHz}$  as well as at  $48.8 \text{ MHz}$ . The highest aspect ratio for a pulse peak fluence of  $0.42 \text{ J/cm}^2$  is obtained at  $6.10 \text{ MHz}$  with  $0.8 \pm 0.2$  and  $9.75 \text{ MHz}$  with  $0.7 \pm 0.2$ . The structures are thus about 1.6 times wider than deep.

Figure 6 a) shows the ablation depths achieved at constant average laser power and varied repetition rates. Shown in Figure 6 b) are the respective aspect ratios of the kerfs. The ablation depth and aspect ratio curves shift to higher values with increasing laser power. For  $24 \text{ W}$ ,  $60 \text{ W}$ ,  $120 \text{ W}$ , and  $240 \text{ W}$ , the current collector is reached in the ablation depth. The highest ablation speed for an ablation to the current collector in one scan is  $5 \text{ m/s}$ . It is reached at  $240 \text{ W}$  and  $48.8 \text{ MHz}$ . The aspect ratio of all channels patterned down to the current collector is lowest at these parameters with  $0.7 \pm 0.1$ . The highest aspect ratio of  $1.55 \pm 0.3$  for ablation down to the current collector is measured at  $24 \text{ W}$  and  $5.42 \text{ MHz}$ . For  $24 \text{ W}$  and  $4.9 \text{ MHz}$ , the aspect ratio drops to  $1.3 \pm 0.2$ .

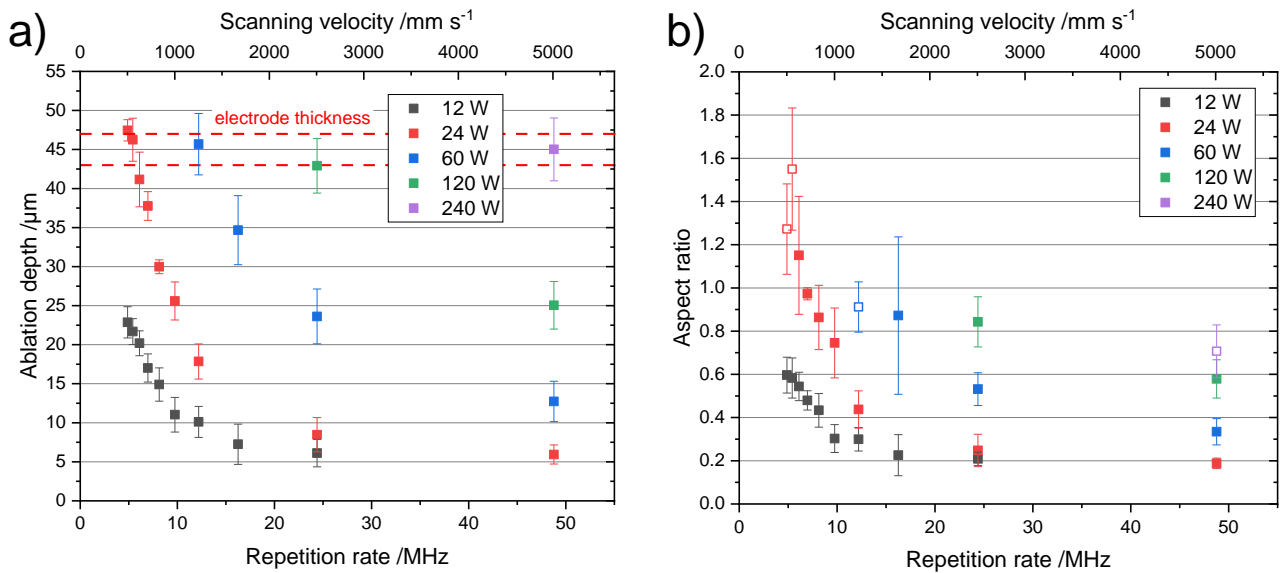


**Figure 6: a) Ablation depth and b) aspect ratio depending on the repetition rate or scanning velocity for constant laser powers. Solid symbols: current collector was not reached, open symbols: current collector was reached.**

**Evaluation of the laser patterning manufactured with “S2” and “S3”**

There is a difference in the depth of ablation achieved with and without the beam splitter, as well as in comparison to “S1”. The depths of removal achieved without beam splitter (“S2”) are significantly greater than for the same structuring parameters with beam splitter (“S3”), as can be seen in Figure 7.

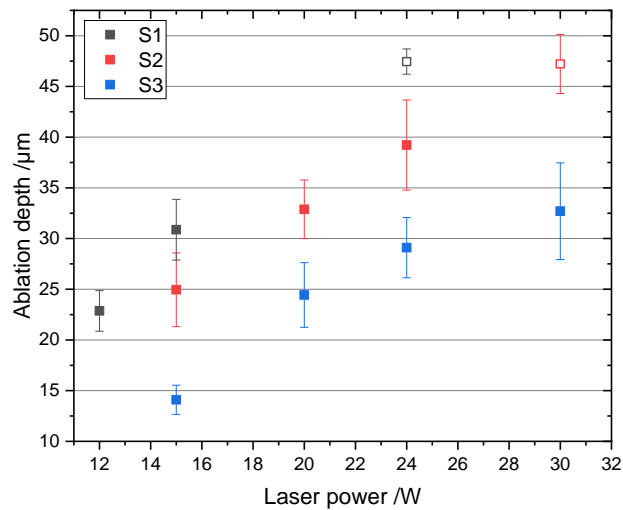


**Figure 7: Ablation depth depending on the laser power for “S1”, “S2” and “S3”. Solid symbols: current collector was not reached, open symbols: current collector was reached.**

Compared with “S1”, in which the current collector is reached at 24 W, 4.9 MHz and 0.5 m/s, in “S2”, this is reached only at a laser power of 30 W. The laser beam has a wider beam waist in “S2”, resulting in lower local intensities and therefore less ablation. The surface of the material appears rugged and cracked in “S2”, indicating thermal influence and suboptimal parameters for laser patterning. The current collector was not reached for “S3”. No significant increase in debris formation can be observed for the structuring with beam splitter compared to structuring without beam splitter, but thermal damage can be seen in the vicinity of the grooves, resulting in a tarnished surface. The power was measured for the total beam, i.e., also the secondary maxima were included in the measurement. The power per beamlet is therefore overestimated.

“S3” can only be compared with “S1” at an average power of 24 W, since in “S1” the measurement series with 20 W and 30 W are faulty. The achieved ablation depths and widths for 24 W, 4.9 MHz and 0.5 m/s are shown in Figure 8 in comparison to the achieved ablation depths and widths in “S1”. In contrast to “S1”, the current collector is not reached in the ablation depth at 24 W in “S3”. The upper ablation width at 24 W in “S1” is 15  $\mu\text{m}$  wider than in “S3”. The middle and lower ablation widths are almost identical. The aspect ratio for “S3” reaches a value of  $0.7 \pm 0.1$ , while the laser structures manufactured with “S1” have an aspect ratio of  $1.2 \pm 0.2$ .

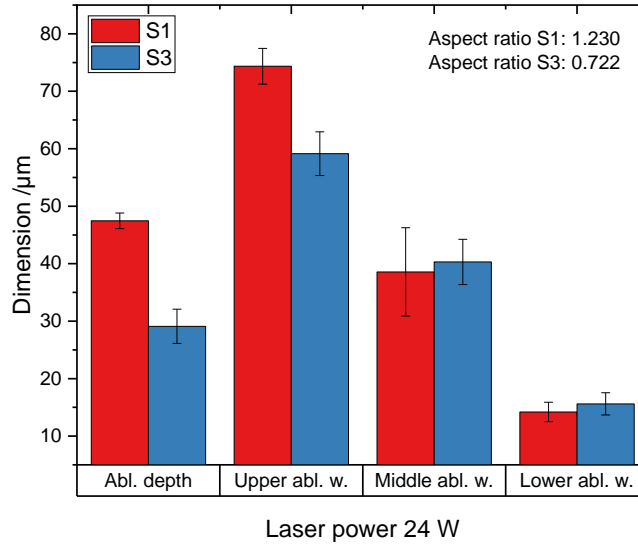


**Figure 8: Ablation depth and widths for “S1” and “S3” at a constant laser power of 24 W, a repetition rate of 4.9 MHz and a scanning velocity of 0.5 m/s.**

The achieved ablation depths and widths with “S2” for 20 W and 30 W can be found in Table 2. Even with an average laser power of 30 W per partial beam, the current collector is not reached.

**Table 2: Ablation widths and depth for “S3” at laser powers of 20 W and 30 W, a repetition rate of 4.9 MHz and a scanning velocity of 0.5 m/s.**

$P_{\text{avg}} / \text{W}$	Abl. depth / $\mu\text{m}$	Upper abl. w. / $\mu\text{m}$	Middle abl. w. / $\mu\text{m}$	Lower abl. w. / $\mu\text{m}$	Aspect ratio
20	$24.4 \pm 3.2$	$59.1 \pm 7.7$	$44.0 \pm 3.6$	$16.5 \pm 2.2$	0.554
30	$32.7 \pm 4.8$	$65.5 \pm 10.3$	$43.1 \pm 4.3$	$21.5 \pm 4.7$	0.759

#### 4. CONCLUSION AND OUTLOOK

In the presented work, the use of an ultrashort pulsed laser system of high power (up to 300 W) and repetition rate (up to 48.8 MHz) was evaluated for laser patterning of commercial anode material representing the state of the art. As part of a parameter study, the repetition rate was varied between 4.9 MHz and 48.8 MHz, the laser feed rate between 500 mm/s and 5000 mm/s, and the average laser power between 6 W and 240 W, while keeping the pulse offset constant.

A transition in ablation behavior, characterized by a change of the slope when the achieved ablation depth was plotted semi-logarithmically versus the pulse peak fluence, was observed. The ablation depths and widths increased with increasing pulse peak fluence. The upper ablation widths of the generated channels increased at constant pulse peak fluence and increasing repetition rate. A patterning velocity of 5 m/s while the current collector was exposed was achieved. However, the generated structures had the lowest aspect ratio of all channels patterned down to the current collector with  $0.7 \pm 0.1$ . The highest aspect ratios were obtained at low repetition rates and high pulse peak fluences.

Since the highest aspect ratio for structuring in “S1” is achieved at the lowest repetition rate, but with a pulse offset of  $0.1 \mu\text{m}$  the current collector is already reached at 24 W, the use of a diffractive beam splitter and/or a beam shaper can be useful. The beam splitter allows the system's maximum laser power of 300 W to be divided among the individual beams. With a required average laser power per individual beam of 24 W at 4.9 MHz (corresponding to a pulse peak fluence of

0.84 J/cm<sup>2</sup> at a repetition rate of 4.9 MHz), the maximum power of the system can be used with a 1x5 beam splitter (with an assumed power loss of less than 17 %). The structuring speed would be increased fivefold in this case.

The cylindrical lens telescope implemented here, in combination with the beam former (“S2”), results in a length of the beam in focus of approx. 270 μm and a width of 65 μm. As a result, the pulse peak fluence decreases by 95 % compared to the pulse peak fluence in “S1” at the same average laser power. By decreasing the pulse peak fluence, the high maximum laser power of 240 W can be used even at low repetition rates without reaching pulse peak fluences at which destruction of the anode would occur at the same pulse overlap. At the same time, the laser feed rate can be increased to reach the same pulse overlap due to the elongated spot.

Structuring in “S2” leads to an ablation characterized by debris formation and fissured channels. The debris and fissures in the generated structures can be reduced by increasing the laser feed rate to over 3.5 m/s. This results in a reduction of the ablation depth.

In contrast to the patterning without beam splitter and shaper, the current collector cannot be reached at the same laser feed rate and repetition rate with “S3”. A maximal ablation depth of 33 μm is observed for an average laser power per beam of 30 W. Due to secondary maxima, the surface of the electrode was tarnished, indicating thermal stress, without generating ablation.

The discolorations and the thermal influence during patterning with the beam splitter could be avoided in a future setup with an adapted scan strategy. The spot spacing could be increased and the pitch could be adjusted by an offset in the size of the desired structure spacing during the next scan. The thermal influence can thus be minimized by increasing the distance between the individual laser beams during patterning compared to blockwise patterning. If the extended optical setup with beam splitter and beam shaper is also to be adapted for anodes with larger layer thicknesses, the pulse peak fluence must be increased. This can be done by increasing the maximum power of the laser system, reducing the repetition rate, or by adapting the cylindrical lens telescope and the associated smaller lengths and widths of the beam in focus. Since at a constant pulse peak fluence the ablation depth increases as the repetition rate decreases, it may be advantageous to increase the pulse peak fluence over decreasing the repetition rate. However, for a given pulse overlap, the laser feed rate must also decrease with decreasing repetition rate. A pulse peak fluence of greater than 1 J/cm<sup>2</sup> can be seen as the target value. A pulse peak fluence of 1 J/cm<sup>2</sup> can be achieved by a repetition rate lower than 1.8 MHz (at a maximum laser power of 200 W) or by increasing the average power of the laser system to about 550 W (assumed without power loss when using the optical elements).

In the framework of the BMBF-project “NextGen-3DBat”, advanced optics, scanners, and lasers have been designed, manufactured, and tested. With the Racoon© 2-axis scan head (Novanta Inc., USA), high precision, low signal processing jitter of 0.5 ps and high processing speed with a full field jump in 9.0 ms for a 21 mm aperture can be realized. In combination with the newly designed F-Theta lens with a large scan field of 150 x 150 mm<sup>2</sup> and a working distance of 255 mm, an aperture of 21 mm and a telecentre angle of 16.8 ° (Sill Optics GmbH & Co. KG, Germany) in combination with optimized beam shaping and splitting (DBS© and FBS-L©, TOPAG Lasertechnik GmbH, Germany), the upscaling of the laser processing can be realized. An ultrafast, high power, high repetition rate laser (FX600-2-GFH©, Edgewave GmbH, Germany) with 600 fs pulse length and a ps-laser with 425 W power at 1 MHz, a pulse length of 12 ps, free trigger pulse repetition rates between single shot and 1 MHz and M<sup>2</sup> of 1.1 (PX600-1©, Edgewave GmbH, Germany) will be used as a laser source, delivering the needed energy for the advanced processing of high-end electrodes.

## ACKNOWLEDGEMENT

This project was funded by the Federal Ministry of Education and Research (BMBF), project “NextGen-3DBat”, under grant number 03XP0198F.

## REFERENCES

- [1] The European Commission – Communication from the commission – The European Green Deal COM2019/640 final (2019).

- [2] Günter, F. J. and Wassiliadis, N., “State of the Art of Lithium-Ion Pouch Cells in Automotive Applications: Cell Teardown and Characterization” *J. Electrochem. Soc.* 169 030515. DOI 10.1149/1945-7111/ac4e11 (2022).
- [3] Pflöging, W. and Pröll, J., “A new approach for rapid electrolyte wetting in tape cast electrodes for lithium-ion batteries”, *J. Mater. Chem. A*, 2, 14918-14926, DOI: 10.1039/C4TA02353F (2014).
- [4] Pflöging, W., “Recent progress in laser texturing of battery materials: a review of tuning electrochemical performances, related material development, and prospects for large-scale manufacturing” *Int. J. Extrem. Manuf.* 3 012002, DOI: 10.1088/2631-7990/abca84 (2020).
- [5] Li, J., Fleetwood, J., Hawley, J. B., and Kays, W., “From Materials to Cell: State-of-the-Art and Prospective Technologies for Lithium-Ion Battery Electrode Processing” *Chem. Rev.* 122, 1, 903–956, DOI: 10.1021/acs.chemrev.1c00565 (2022).
- [6] Nolte, S., Momma, C., Jacobs, H., and Tünnermann, A., “Ablation of metals by ultrashort laser pulses” *J. Opt. Soc. Am. B/Vol. 14*, No. 10 (1997).